Engineering Structures 337 (2025) 120445

Contents lists available at ScienceDirect

Engineering Structures

journal homepage: www.elsevier.com/locate/engstruct

Advances in fatigue design of circumferential welds in offshore wind turbine monopile support structures

Ali Mehmanparast [a,*], Inge Lotsberg [b]

[a] Department of Naval Architecture, Ocean and Marine Engineering, University of Strathclyde, Glasgow G1 1XQ, United Kingdom
[b] Det Norske Veritas (DNV), Veritasveien 1, 1363Høvik, Norway

ARTICLE INFO

Keywords:
Fatigue design life
Monopile foundations
Circumferential welds
Offshore wind turbines
Structural integrity

ABSTRACT

The increasing trend in size and thickness of offshore wind turbine monopile support structures necessitates the need for continued research to refine fatigue design methodologies by ensuring both structural integrity and cost-effectiveness. This study investigates fatigue life predictions at the circumferential welds in monopile foundations by performing a detailed analysis of the SLIC fatigue data, obtained from 50 mm thick as-welded specimens, and incorporating realistic weld geometries in the evaluations. Moreover, comparisons are drawn between the monopile-specific D curve introduced in the new edition of the DNV-RP-C203 standard, the generic D curve, and the processed SLIC data. The results show that, at a reference thickness of 25 mm, the new monopile-specific D curve mitigates the over-conservatism of the generic D curve, which is designed for a wide range of applications, resulting in 3.3 times increase in fatigue life at 10^7 cycles. Furthermore, the results from sensitivity analyses performed by accounting for variations in weld geometry demonstrate the critical importance of precise weld geometry characterisation in evaluating S-N fatigue data. Additionally, the findings from this research underscore the critical role of residual stresses in the fatigue design and life assessment of in-service monopiles. The advancements presented in this study contribute to better understanding of the fatigue life in large thickness monopile support structures. The findings from this study not only aid in re-evaluating the fatigue life of aging offshore wind turbine monopiles but also contribute to designing longer-lasting foundations for future installations.

1. Introduction

Offshore wind has been globally recognised as a reliable source of clean energy to realise the short-term and long-term energy demands and facilitate the pathway for transition towards clean and low emission energy sources. The very first commercial offshore wind farm in the world was commissioned in Denmark in 1991 in shallow water of 2–6 m deep, which included 11 offshore wind turbines (OWTs) and the total capacity of 5 MW, with the first major offshore wind farms in Europe commissioned in early 2000s [1]. Nowadays, offshore wind has evolved into a global industry, with nations competing to harness this clean energy. Recent cost reductions in particular have driven rapid growth, with fixed-bottom offshore wind now cheaper than gas at under €40/MWh in the UK and Europe [2]. The UK was the first major economy to set a legally binding net-zero emissions target followed by the EU's climate neutrality goal, both by 2050 [3,4]. UK and EU aim to expand their installed offshore wind capacity to 60 GW and 111 GW, respectively, by 2030 [5,6]. To meet the 2050 net-zero goal, the UK requires 125 GW of offshore wind capacity, while the EU targets 317 GW [5,6]. The current installed offshore wind capacity, until end of 2024, is around 35 GW in Europe, which includes 15 GW of installed capacity in the UK, producing electricity from over 2700 OWTs, and another 20 GW in the EU from over 6500 installed OWTs [7].

In order to maintain the exponential growth of offshore wind installations in Europe, it is essential to identify and address the engineering challenges associated with these large-scale structures, which are continuously growing in size and thickness as a result of larger wind turbine capacities and bigger rotor diameters. During their lifetime these structures are subject to cyclic loading conditions causing fatigue damage. The foundations in particular are subject to severe environmental (wave, wind and current) and operational (rotation of the turbine) loads. Therefore, engineering considerations must be carefully implemented to design them against fatigue failure. Considering the typical design life of 20–25 years, large volumes of the fast-aging OWTs

* Corresponding author.
E-mail address: ali.mehmanparast@strath.ac.uk (A. Mehmanparast).

https://doi.org/10.1016/j.engstruct.2025.120445
Received 13 January 2025; Received in revised form 1 April 2025; Accepted 23 April 2025
Available online 12 May 2025

are nearing their end of initial design life within the next decade, hence appropriate decisions must be made regarding life-extension, repowering or decommissioning. In the UK alone the number of OWTs to reach the end of their initial design life within the next decade is nearly 1200 (see Fig. 1) with a similar number in the EU. To sustain growth in offshore wind capacity and reduce costs, it is crucial to safely extend the operation of existing turbines beyond their design life wherever possible and also design the new installations for longer operational lives. However, this requires a deep understanding of fatigue design and quantified levels of conservatism in current design curves. Knowing that the levelized cost of energy (LCoE) is a function of operational life, any increase in the life of OWTs will deliver positive impact and incentivise investors to further contribute to this profitable business [8].

Depending on the water depth and distance from the shore there are different types of OWT foundations which are commonly employed in design of offshore wind farms. As shown in Fig. 2(a), until the end of 2024 83 % of the existing OWTs in the UK are supported using monopile foundations in relatively shallow water depths, with much lower percentage of 16 % supported using jacket structures in larger water depths, and 1 % of the remaining OWTs supported using other types of foundations, including gravity base, suction buckets and floating spars. This figure shows that monopile foundations, which are relatively easier to fabricate, are currently the preferred solution for deployment of offshore wind farms. These structures are constructed by bending and cold-forming thick structural steel plates into cylindrical shapes, which are then welded along their longitudinal edges. Subsequently, these large-diameter hollow cylinders are circumferentially welded (as illustrated in Fig. 2(b)) to achieve the full design length of the monopile [9]. During installation, the monopiles are subject to intense hammering loads to drive a portion of their total length into the seabed, while the remaining section extends to the water level, where the transition piece is mounted on top. During the operational phase, lateral cyclic forces acting on the structure from wind and waves generate global cyclic bending moments in the monopiles with resulting axial stress ranges, promoting the initiation and propagation of fatigue cracks, particularly at the circumferential welds, as schematically shown in Fig. 2(b). The welded sections are more susceptible to failure due to factors such as geometrical mismatches, variations in grain size and microstructure, higher localised stresses at the weld toes, and the possible presence of weld defects and damaging tensile residual stresses.

The purpose of the present study is to build a better understanding of the fatigue design life of OWT monopiles with the focus on the circumferential welds. This knowledge will help the designers and operators to implement knowledge-based engineering judgements, on top

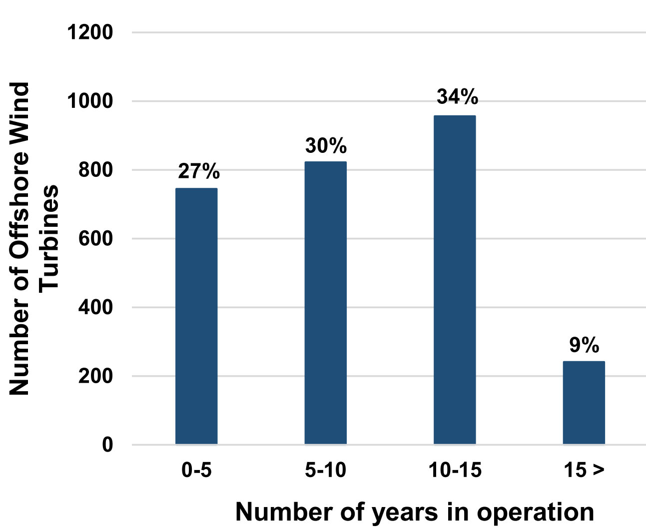

Fig. 1. Age distribution of OWT installations in the UK until end of 2024.

of the generic guidelines provided in international standards, to improve the longevity of the offshore wind infrastructure. Since international standards establish fatigue design curves for butt welds based on reference thicknesses significantly smaller than those of monopiles, this study provides valuable insights into the fatigue behaviour of thicker welds. The aim of this study is to develop a fundamental understanding to reduce excessive conservatism in fatigue design curves, thereby extending the lifespans of aging monopiles (which are up to 100 mm thick) and new designs with thicknesses up to 170 mm.

2. Recommended fatigue design curves in international standards

There are a few major international standards, which specify recommendations for fatigue design of welded structures. The most widely used standards for industrial applications are (a) “API Recommended Practice 2A-WSD: Planning, designing, and constructing fixed offshore platforms—working stress design” [10], (b) “EN 1993-1-9-Eurocode 3: Design of steel structures” [11], (c) “BS 7608: Guide to fatigue design and assessment of steel products” [12], and (d) “DNV-RP-C203: Fatigue design of offshore steel structures” [13]. The reference thickness for S-N fatigue design of butt-welded plates specified in Eurocode, BS and DNV standards is 25 mm, which is much smaller than the typical thickness range in monopiles. It is worth noting that EN 1993-1-9-Eurocode 3 only provides recommended fatigue design curves in air while BS 7608 explicitly states that this British Standard is not applicable to fixed offshore structures. Among these standards, DNV-RP-C203 is widely used in the design of OWT monopile foundations due to the coverage of wide range of offshore welded structures and consideration of various environments, including air, seawater with cathodic protection and seawater with free-corrosion environment.

There are series of fatigue design curves provided for various types of welded structures with different weld quality and surface finish (e.g. with or without grinding the weld toe) in DNV-RP-C203 standard. The curve that is often employed in the design of OWT monopile foundations is the D curve, which is associated with the double V-groove multi-pass transverse butt welds under axial loading. This curve is often utilised for the design of monopiles by considering as-welded condition without any post-weld surface finish or heat treatment. Although OWT monopile foundations are protected against corrosion throughout most of their operational lifecycle using cathodic protection and coating, the fundamental understanding of their fatigue behaviour in a seawater environment is derived from the baseline fatigue design curve in air environment in conjunction with limited historical test data in seawater environment with cathodic protection and free-corrosion conditions. Therefore, the first step to make suitable engineering judgments for design of monopiles is to comprehensively understand the assumptions and limitations behind the recommended D curve in air, which is provided in DNV-RP-C203 standard.

2.1. Comparison of the generic and monopile-specific D curves in DNV-RP-C203

A new edition of DNV-RP-C203 standard was released recently, in October 2024 [13]. In this edition, the generic D curve remains in the main body of the standard, unchanged from the previous edition [14]. Additionally, a new appendix has been introduced, titled “Appendix F.16: S-N curves for high-quality butt welds in large-diameter wind turbine support structures”. This appendix, which was developed using the latest fatigue test data relevant to monopiles, aims to provide more refined design curves for large-diameter OWT monopile welded structures. The curves in this appendix are based on a new constant amplitude fatigue dataset on 50 mm thick as-welded samples (detailed in Section 3.1, with the raw fatigue test data summarised in Appendix A) for the first part of the S-N curve, supplemented by fracture mechanics analysis for the second part of the S-N curve where the fatigue limit is observed in

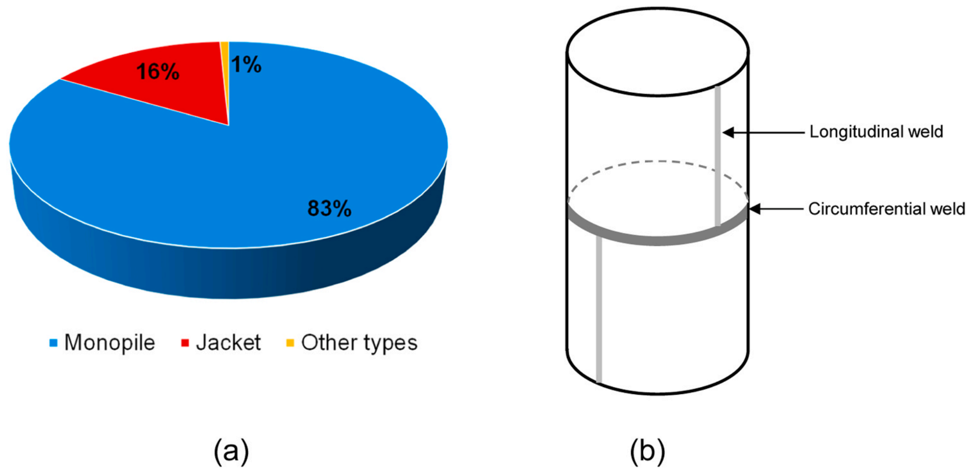

Fig. 2. (a) Percentage distribution of the OWT foundation types for the currently installed offshore wind farms in the UK until end of 2024, (b) Schematic illustration of longitudinal and circumferential welds in monopiles.

constant amplitude tests. As stated in this appendix, the monopile-specific D curves are provided for air and seawater with cathodic protection condition, while the generic D curve in free-corrosion environment presented in the main body of the standard is recommended for the seawater environment without cathodic protection. The background information on derivation of this monopile-specific S-N curve can be found in [15].

As explained in DNV-RP-C203 standard [13], the S-N fatigue design curve can be defined by correlating the number of cycles to failure, *N*, with the stress range, $\Delta\sigma$ (which is also conventionally referred to as *S*) with unit in MPa, using a power-law equation, which can be described in log-log scale using Eq. 1:

$$\log N = \log\bar{a} - m\log\Delta\sigma \tag{1}$$

where *m* is the inverse slope of the S-N curve and $\log\bar{a}$ is the intercept of the design S-N curve with the log *N* axis, which can be derived from:

$$\log\bar{a} = \log a - 2s_{\log N} \tag{2}$$

where $\log a$ is the intercept of the mean S-N curve with the log *N* axis, and $s_{\log N}$ is standard deviation (SD) of log *N*. In other words, the intercept of the design curve can be calculated as the intercept of the "mean-2SD" curve. It has been recommended in DNV-RP-C203 standard to take a typical value of $s_{\log N}= 0.2$ for welded connections in the absence of test data for a specific design and fabrication. It is worth noting that the inverse slope of the S-N fatigue design curve is always negative, this is why the DNV standard presents the equation with *-m* to make the equation easier to utilise by the general users. The recommended fatigue design curves provided in DNV-RP-C203 standard are presented in a bi-linear format in log-log axes, where the subscript 1 is used to describe the inverse slope m_1 and intercept $\log\bar{a}_1$ in the low-cycle (i.e. high-stress range) region and subscript 2 is used to describe the inverse slope m_2 and intercept $\log\bar{a}_2$ in the high-cycle (i.e. low-stress range) region to the right of the constant amplitude fatigue limit.

The generic D curve in air provided in the latest edition of DNV-RP-C203 standard, which is the same as the one presented in the previous edition of the standard [14], hence denoted "D curve-Air-DNV2021 (Generic)" in the present study, and the monopile-specific D curve in air [13], denoted "D curve-Air-DNV2024 (Monopile)" in the present study, are plotted and compared with each other in Fig. 3(a) for the reference thickness of $t_{ref} = 25$ mm, with the S-N design curve parameters summarised in Table 1. As seen in Fig. 3(a) and Table 1, the low and high-cycle inverse slopes of $m_1= 3$ and $m_2= 5$, respectively, for the generic curves have been revised to $m_1= 3.45$ and $m_2= 5.7$ for the monopile-specific D curve in air. Moreover, the low and high-cycle

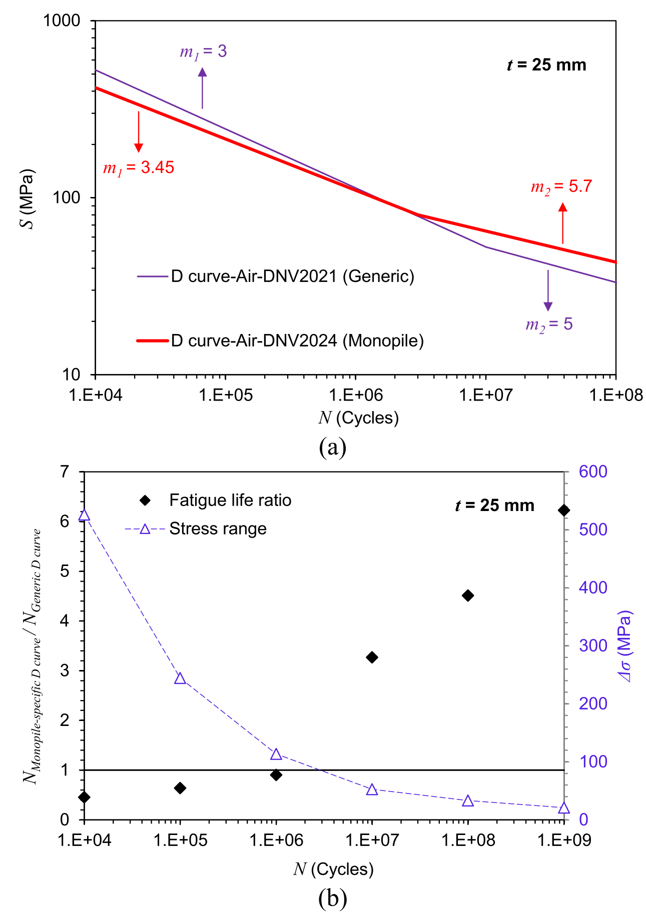

Fig. 3. (a) Comparison of the generic and monopile-specific D curves in air specified in DNV-RP-C203, (b) Comparison of the ratio of fatigue lives calculated from the monopile-specific D curve over the generic D curve across various cycle counts, for the reference thickness of 25 mm.

intercepts of $\log\bar{a}_1= 12.164$ and $\log\bar{a}_2= 15.606$, respectively, for the generic curves have been revised to $\log\bar{a}_1= 13.043$ and $\log\bar{a}_2= 17.325$ for the monopile-specific D curve in air. Lastly, the change-over point of $N_t= 10^7$ cycles between the inverse slopes of m_1 and m_2 in the generic D curve in air has been revised to $N_t= 3 \times 10^6$ for the monopile-specific D curve. The comparison of the two design curves in Fig. 3(a) shows that

Table 1
Generic and monopile-specific fatigue design D curve constants provided in DNV-RP-C203 standard.

	m_1	$\log\bar{a}_1$	m_2	$\log\bar{a}_2$	N_t
D curve-Air-DNV2021 (Generic)	3	12.164	5	15.606	10^7
D curve-Air-DNV2024 (Monopile)	3.45	13.043	5.7	17.325	3×10^6

the use of generic D curve for monopile applications can result in non-conservative fatigue design in the low-cycle (i.e. high-stress) region with $N < 3 \times 10^6$ cycles and over-conservatism in the high-cycle (i.e. low-stress) region with $N > 3 \times 10^6$.

The comparison of the ratio of fatigue lives calculated from monopile-specific D curve over generic D curve across various number of cycles is presented in Fig. 3(b), for the reference thickness of 25 mm. The non-conservatism in fatigue life calculation from the generic D curve for $N < 3 \times 10^6$ and over-conservatism for $N > 3 \times 10^6$, compared to the monopile-specific D curve, is illustrated in this figure. As seen in Fig. 3 (b), for the reference thickness of 25 mm, at the number of cycles to failure of $N = 10^7$ from the generic D curve in air the fatigue design life would be 3.3 times longer by employing the monopile-specific D curve at the same stress range level (i.e. $\Delta\sigma = 52.63$ MPa). In other words, at this stress range level, the design life of 20 years based on the generic D curve would increase to 66 years based on the monopile-specific D curve. This highlights the fact that while the fatigue damage at high-stress range levels can be under-predicted by employing the generic D curve in air, the number of cycles to failure can be significantly under-estimated when the generic D curve is employed in calculations compared to the monopile-specific D curve. It can be added here that the main contribution to calculated fatigue damage in a monopile structure is for stress ranges in the S-N curve from 10^6 – 10^8 cycles for a typical long term stress range distribution [15]. Thus, to assess factor on improvement for actual structures it is necessary to consider relevant long-term stress range distributions and difference regarding fabrication tolerances built into the two S-N curves as explained in [15]. One needs also to consider the fatigue damage consumed in pile driving, which will be different when using the monopile-specific S-N curve in the latest version of DNV-RP-C203 standard, compared to the generic D curve. Moreover, any effort to optimise the thickness of future monopile designs must account for both buckling and fatigue. While reducing thickness in future designs can lower the capital expenditure (CAPEX), there is a risk of shifting the failure mechanism from fatigue to buckling if careful engineering considerations are not incorporated into the optimisation process.

While the standard design curves for butt welds are provided for the reference thickness of $t_{ref} = 25$ mm in DNV-RP-C203, an equation has been provided to modify the design curves for the butt welds with thicknesses of $t > 25$ mm, using Eq. 3:

$$\log N = \log\bar{a} - m\log\left(\Delta\sigma\left(\frac{t_{eff}}{t_{ref}}\right)^k\right) \tag{3}$$

where k is a thickness exponent, which is equal to 0.2 for the D curve in air, and t_{eff} is the effective thickness which can be defined using Eq. 4:

$$t_{eff} = Min[(14 + 0.66L_t),\ T] \tag{4}$$

where L_t is the weld width and T is the plate thickness, as schematically shown for a double V-grooved butt-weld under axial tensile stress in Fig. 4. More details about the weld width effect on fatigue life can be found in [16]. It is worth noting that in the previous edition of DNV-RP-C203 standard [14] the definition of the weld width was given as the distance between the two weld toes on the side of the double V-grooved butt-welded plate. However, in the monopile-specific appendix of the latest edition of the standard [13] it has been recommended to add $\Delta h = 3$ mm on each side of the width of the weld groove

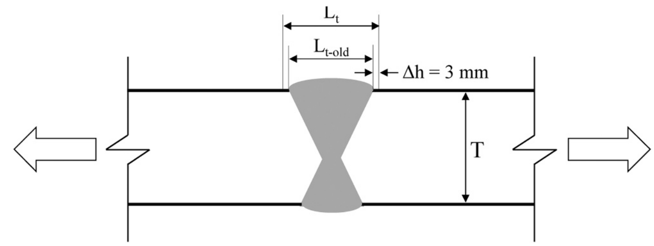

Fig. 4. Schematic illustration of the weld width and plate thickness in a double V-grooved butt-weld.

(see Fig. 4) to quantify the L_t value. In order to differentiate between two different approaches to determine the weld width parameter, in this study the original definition used for the generic D curve analysis, that is the same as the previous edition of the standard, is denoted L_{t-old}, while the monopile-specific definition is described as L_t using Eq. 5 as also shown in Fig. 4:

$$L_t = L_{t-old} + 2\Delta h \tag{5}$$

The final consideration that must be taken into account in calculation of the design curve for as-welded monopiles is the influence of the weld length on the number of cycles to failure, which may affect the probability of weld defects and cracking. According to DNV-RP-C203 guidelines, the influence of the weld length of the fatigue design curves can be described using Eq. 6 for the first part (i.e. high-stress region) of the S-N curve:

$$\log N = \log\bar{a}_1 - m_1\log\left(\Delta\sigma\left(\frac{t_{eff}}{t_{ref}}\right)^k\right) - \frac{s_{\log N}}{2}\log\left(\frac{L_{weld}}{l_{weld-ref}}n_s\right) \tag{6}$$

where n_s is the number of similar connections subjected to the same stress range, L_{weld} is the length of weld subjected to the same stress range, $l_{weld-ref}$ is the reference weld length which corresponds to a typical weld length valued in the test specimens employed in derivation of S-N curve. It has been recommended in DNV-RP-C203 standard to take the reference value of the weld length as $l_{weld-ref} = 100$ mm.

The effect of weld length on the fatigue design curve can be described using Eq. 7 and Eq. 8 for the second part of the S-N curve (the low-stress region):

$$\log N = \log\bar{a}_2 - m_2\log\left(\Delta\sigma\left(\frac{t_{eff}}{t_{ref}}\right)^k\right) \tag{7}$$

$$\log\bar{a}_2 = \frac{m_2}{m_1}\left(\log\bar{a}_1 - \frac{s_{\log N}}{2}\log\left(\frac{L_{weld}}{l_{weld-ref}}n_s\right)\right) + \left(1 - \frac{m_2}{m_1}\right)\log N_1 \tag{8}$$

2.2. Motivation for further research

As it is evident from the recommendations in DNV-RP-C203 standard, the historical fatigue tests employed in derivation of the design curves for butt welds were carried out decades ago on specimens with thicknesses mostly less than 25 mm. Subsequently, the reference thickness for the derived S-N curves in DNV-RP-C203 standard was chosen to be 25 mm, which is much smaller than the thickness range of the current and future generation of OWT monopile foundations. Therefore, there is need to examine suitability of the recommendations for fatigue design of thicker welded structures and explore the sensitivity of the proposed methodologies to the variations in realistic weld parameters observed in actual large thickness welded monopiles. Moreover, while the previous edition of DNV-RP-C203 [14] was proposing over-conservative fatigue design curves for the as-welded condition (see Fig. 3) in the high-cycle region, the new edition of the standard [13] has attempted to reduce the level of conservatism for design of monopiles, which subsequently enables re-analysing the remaining life of the existing OWT infrastructure and enhances the longevity of the future generation of monopiles with even larger thicknesses. However, there is still need for carrying out data-informed sensitivity analyses to examine the sufficiency of the level of conservatism in the new monopile-specific D curve in air specified in the new edition of DNV-RP-C203 standard, which forms the core objective of this study. Also, another important motivation for performing the present study is to explore the impact of less conservative assumptions, compared to the ones originally employed in derivation of S-N curves (such as assuming high magnitude tensile residual stresses at the circumferential welds of monopiles during the entire lifecycle), which will give more flexibility to designers and operators to make informed engineering judgments for the asset management of their OWT structures.

3. Fatigue behaviour in large thickness SLIC specimens

3.1. SLIC project

To address the knowledge gaps and improve the best practice in fatigue design of OWT monopile foundations, the Structural Lifecycle Industry Collaboration Joint Industry Project (SLIC JIP) was established a few years ago. This initiative yielded significant outputs, including material characterisation [17], fracture mechanics database [18], uniaxial fatigue database on thick welded samples [19], by replicating the welding condition and procedure employed in fabrication of monopiles. The uniaxial fatigue testing in the SLIC project involved large-scale dog-bone shaped specimens with approximate dimensions of $T = 50$ mm in thickness, $L_{weld} = 100$ mm in width, and a total length of 1.5 m. The material used for the S-N fatigue round-robin test programme, with multiple monopile fabricators and test centres involved in it, was EN10025–4:2004 S355ML structural steel [20], a standard choice in the fabrication of OWT monopiles. During production, double V-grooved steel plates were joined through multi-pass butt welding, following established industry procedures for monopile fabrication. Post-welding inspections were conducted to rigorously assess misalignment angles and welding defects, ensuring that only welded plates conforming to offshore wind industry standards were selected for testing.

Large dog-bone specimens were extracted with the loading axis oriented perpendicular to the weld direction, maintaining the as-welded condition without grinding the weld toe. Strain gauges were attached to both sides of each specimen to account for misalignment in the analysis. Due to the very large cross-sectional area in test specimens, 2.5 MN testing machines were utilised for fatigue testing to achieve the target load levels. All tests were performed in air under constant-amplitude cyclic loading, using load-control mode with a load ratio of $R = 0.1$. This loading condition has been historically used in test programs over the past few decades to derive the S-N curves in the high-stress range region [19]. Despite the technical challenges and high costs associated with fatigue testing of large thickness welded specimens, 31 tests were successfully conducted in the SLIC project on as-welded samples, the results of which are summarised in Appendix A. Of these, 29 tests were carried out to failure (defined as full-width crack formation), while 2 tests, which showed no signs of crack initiation, were classified as run-outs and excluded from the linear regression analyses of the test data.

All of the uniaxial specimens tested throughout the SLIC JIP were thoroughly characterised before and after testing to quantify the variation in the weld parameters across 29 as-welded samples, which were tested to completion. The variations in these parameters are summarised in Table 2, where the average, maximum and minimum values are reported for each of these parameters. The weld parameters listed in this table include the weld width normalised by the thickness, L_t/T, the weld length normalised by the thickness, L_{weld}/T, and the notch stress concentration factor at the weld toe (SCF), which is often shown as K_t. These data in Table 2 provide a very important source of information for further fatigue analysis, which is presented in the following sections, and also build a reliable source of well-categorised information for any fatigue related analyses that will be carried out by other researchers in the future.

Table 2
Characterisation of weld parameters in as-welded SLIC samples which were tested to completion.

	L_t/T	L_{weld}/T	K_t
Average	1.04	1.98	1.98
Minimum	0.84	1.96	1.42
Maximum	1.20	2.01	2.70

The determination of the notch stress concentration factor K_t for each of the as-welded SLIC samples was carried out using the laser scanning technique in conjunction with finite element analysis. By utilising high-resolution 3D laser scanning technique, weld geometries were captured and imported into a finite element software for further analysis. A thorough mesh sensitivity analysis was conducted to refine the mesh at the weld toe, and the ratio of notch stress to nominal stress was evaluated. The K_t values were averaged over ten measurements along the width of each sample to account for welding quality and material variability. This procedure effectively captured accurate notch stress concentration factors, reflecting the variability inherent in real-life monopile welds and providing highly representative data.

3.2. Analysis of the SLIC raw data

The results from linear regression analysis on the SLIC raw data obtained from 29 completed uniaxial fatigue tests (without including 2 run-outs) were presented in [19] and are summarised in Table 3. It is important to note that the stress range data which is presented and analysed in [19] included the weld misalignment factor, which was individually measured using strain gauges for each of the samples tested in the SLIC project (see Section 3.1). It is also worth noting that the data presented in [19] were not modified by any size factor neither weld parameters such as L_t and L_{weld}, which is the procedure described in DNV-RP-C203 and briefly explained in Section 2.1, hence why the terminology that is used here is the SLIC raw data. In other words, the results presented in Table 3 are derived directly from the SLIC raw data, without any adjustments for thickness correction or weld geometry. A comparison of the results from the raw data in Table 3 and the standard design curves in Table 1 shows that the inverse slope of $m = 3.37$ obtained from SLIC raw data falls between m_1 values of 3 and 3.45, which are included in the latest edition of DNV-RP-C203 standard for generic (which is the same D curve included in the previous edition of the standard) and monopile-specific D curves, respectively. Further analysis using a Bayesian regression model, which was based on data sampling by including a mathematical function to consider the 2 run-out data points, in [19] showed that an inverse slope of $m = 3.5$ can be obtained from more advanced statistical approaches. It has been explained in [15] that the regression analysis on the SLIC data, in conjunction with the fatigue database at other thicknesses available to DNV, was the basis of the first part (i.e. low-cycle region) of the new monopile-specific D curve which is represented in the new edition of DNV-RP-C203 standard [13]. In order to better understand the influence of thickness and weld parameters on the fatigue design curve, various analyses have been carried out in the following section to evaluate the sensitivity of the fatigue curves to each of the key parameters specified in DNV standard.

Table 3
Summary of the linear regression analysis results obtained from 29 completed fatigue tests in the SLIC project, taken from [19].

m	$\log\bar{a}$	$\log a$	$s_{\log N}$	R^2
3.37	12.786	13.210	0.208	0.82

3.3. Sensitivity analysis of the SLIC data to various correction factors

As outlined in Section 2.1, the effect of thickness on fatigue life reduction in S-N curves can be estimated using Eq. 3, as recommended in DNV-RP-C203 standard. This equation incorporates the thickness T, weld width L_t and weld length L_{weld} parameters, with their impact on the shift in the S-N curve defined by Eq. 4-Eq. 8. In this section, the thickness correction methodology detailed in DNV-RP-C203 is applied to the SLIC data (which have $t > 25$ mm) to directly compare them with the thickness corrected D curves. The realistic values of the weld parameters obtained by characterising 29 as-welded SLIC samples, reported in Table 2, were employed in further analyses of the S-N fatigue results, which are shown and discussed below. It is worth noting that in the analyses below, "processed" data refers to SLIC "raw" data that has been adjusted using weld geometry parameters in accordance with the guidelines outlined in DNV-RP-C203 (see Section 2.1).

3.3.1. Applying the average value of L_t to all data points

The first set of analysis was carried out by employing a fixed value of L_t parameter obtained from the average value of weld widths across 29 completed tests in the SLIC project (see Table 2) in calculation of t_{eff} (see Eq. 3, Eq. 4 and Eq. 5) for each of the 29 test data points. The result from this analysis, which was carried out in accordance to Eq. 3 with the fatigue life on the Y-axis and $\Delta\sigma\left(\frac{t_{eff}}{t_{ref}}\right)^k$ on the X-axis, is shown in Fig. 5(a) and the regression parameters together with $s_{\log N}$ and R^2 values are summarised in Table 4. Also included in this Figure are the SLIC raw data and the associated regression lines without any data processing. In this table $s_{\log N}$ indicates the level of scatter in the data while R^2 shows the level of accuracy of the line of best fit made to the data points. Moreover, the obtained results from the regression analysis on the processed data are compared with the generic and monopile-specific thickness corrected DNV design curves in Fig. 5(b). It is worth noting that based on the recommendations in the latest edition of DNV standard [13], $\Delta h = 3$ was incorporated in calculation of L_t parameter for the SLIC data as well as the monopile-specific D curve specified in 2024 edition of the standard, while L_{t-old} parameter was used for calculating the generic D curve which is based on the descriptions provided in the previous edition of the standard from 2021. Moreover, the average value of thickness T across 29 SLIC specimens was employed in the analysis of the test data as well as design curves. As seen in Fig. 5(a) and Table 4, applying a fixed value of weld width L_t does not change the inverse slope, $s_{\log N}$, and R^2 values compared to the linear regression analysis results from the SLIC raw data presented in Fig. 5(a) and Table 3, and only influences the mean and mean$\pm$ 2 SD intercepts. Also seen in Fig. 5 (b) is that the generic D curve, based on the 2021 edition of the DNV standard, is found non-conservative for mean-2SD line obtained from the processed SLIC data in the high-stress range region, while the monopile-specific D curve provided in the latest edition of the standard is found to be suitably conservative for the entire stress range levels obtained from the processed SLIC data.

3.3.2. Applying individual values of L_t to each data point

After examining the influence of a fixed value of L_t on data processing, the influence of variable values was examined by applying individual weld width L_t and specimen thickness T values to calculate the effective thickness t_{eff} for each of the SLIC data points. The result from the regression analysis based on this data processing strategy is presented in Fig. 6(a), with the intercept and inverse slope values summarised in Table 4. Also included in this Figure are the SLIC raw data and the associated regression lines without any data processing. The comparison of the processed data and the associated regression lines with the generic and monopile-specific thickness corrected D curves is shown in Fig. 6(b). The results in Fig. 6(a) and Table 4 show that by employing the specific values of weld width and specimen thickness in

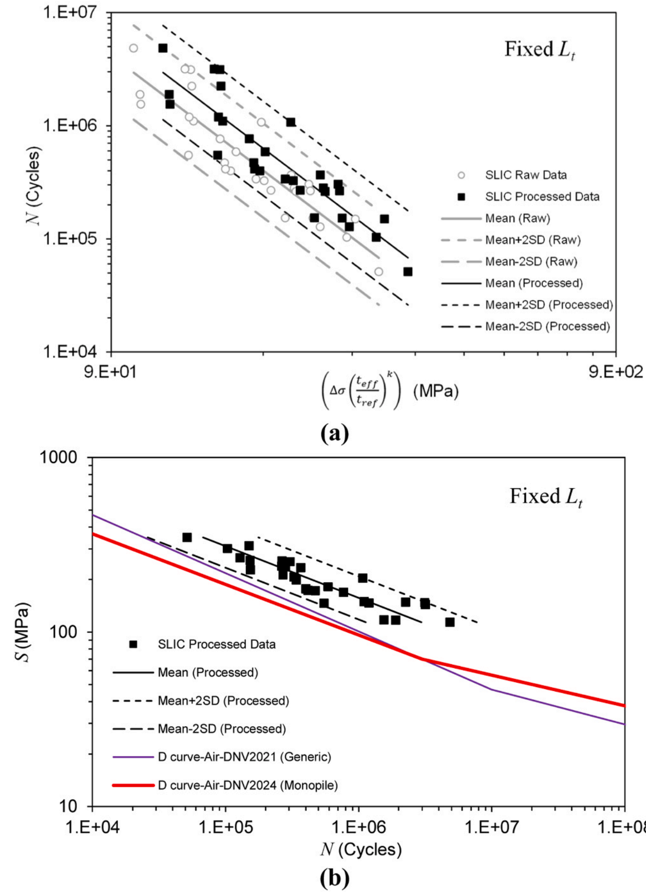

Fig. 5. (a) Comparison of the SLIC raw data with the processed data using the fixed L_t parameter obtained from the average weld widths across 29 completed tests, (b) comparison of the regression lines from the processed SLIC data with the fatigue design curves obtained from the old and new editions of DNV-RP-C203 standard.

data analysis the magnitude of the inverse slope increases while the SD reduces and R^2 increases compared to the fixed L_t scenario. This indicates that when individual values of L_t and T parameters are used in data analysis, the level of scatter reduces and the accuracy of the line of best fit improves compared to the SLIC raw data presented in Fig. 6(a) and Table 3, and the SLIC processed data based on the fixed L_t assumption presented in Table 4 (see 3.3.1). Furthermore, it can be observed in Fig. 6(b) and Table 4 that the obtained inverse slope of $m = 3.43$ from this data analysis procedure is very close to the monopile-specific D curve value of $m = 3.45$. Last but not least, Fig. 6(b) shows that the generic design D curve is found non-conservative in the high-stress range region compared to mean-2SD line from the processed SLIC data, while the monopile-specific D curve is found conservative across the entire data set.

In order to further analyse this data processing strategy, the analysis was repeated by fixing the inverse slope to the monopile-specific value of $m = 3.45$ provided in the latest edition of the standard and the rest of the regression parameters were recalculated and reported in Table 4. As seen in this table, fixing the inverse slope and using the same data processing strategy, by employing variable weld width L_t and specimen thickness T values across different specimens, does not change the values of SD and R^2 and only the mean and mean-2SD intercept values change very slightly compared to the free slope scenario. Comparison of the $\log\bar{a}$ parameter obtained from this analysis, with that of reported for monopile-specific D curve in Table 1 shows that the intercept value from the processed SLIC data falls very close to the monopile-specific design curve provided in the latest edition of the standard, with the design curve being slightly more conservative compared to the mean-2SD curve from the processed SLIC data with a fixed slope of 3.45.

3.3.3. Examination of new formulations for thickness effects on S-N curves

To further evaluate the thickness effects on the S-N fatigue design curves, a range of new equations with similar structures as the ones provided in DNV-RP-C203 standard (see Eq. 3-Eq. 6) were considered, which are summarised in Table 4. In this sensitivity analysis, a number of stress-range multipliers (SM) are examined in the analysis of the SLIC data to evaluate their effectiveness compared to the original stress range coefficient of $\left(\frac{t_{eff}}{t_{ref}}\right)^k$ that has been provided in the standard. To find the solutions for the variable D that is introduced into the new equations, an iterative process was established based on the least squares method, to find the optimum value by minimising the sum of the squared residuals.

As seen in Table 4, the equations for SM1—6 have the same structure as the current stress range coefficient available in DNV standard, with variable D embedded in different parts of the equation. As seen in this table, the constants that are recommended in Eq. 4 and Eq. 5 are relatively sensitive to the database and the optimum values obtained solely using the SLIC database are somewhat different to those recommended in the standard. It can be seen in this table that for 50 mm thick SLIC data points the optimum solution for L_t coefficient, which results in the lowest value of SD, is found to be 0.6 instead of 0.66 that is originally implemented in the standard while it has been also found in SM2 that replacing the constant of 14 with 0 would reduce the SD and increases the R^2. It can be also seen in this table that in the absence of constant 14 in the formulation of t_{eff} a coefficient of 0.8 for L_t parameter can reduce the SD using SM3 equation. Moreover, reducing the value of Δh to 0 and introducing a multiplier with the value of 1.11 for T in the definition of t_{eff} have been found to decrease the SD value. Finally, for this general form of equation which defines t_{eff} it can be seen that an exponent of larger than 0.2 which is currently recommended in the standard can further reduce the scatter level by analysing solely the SLIC data. It is quite important to note that using different optimum values of constants in the general form of t_{eff} equation, which are shown in SM1—6, the monopile-specific D curve falls below mean-2SD line from the processed SLIC data, hence the monopile-specific design curve is found to be sufficiently conservative for design purposes despite sensitivities to various assumptions and weld parameters.

To better understand the effect of K_t on fatigue life, the SLIC raw notch stress range data (i.e. where the notch stress range at the weld toe is calculated as the nominal stress multiplied by K_t) is compared with the recommended notch stress S-N curve in Appendix E of DNV-RP-C203 in Fig. 7. As mentioned in DNV-RP-C203, the curve in Appendix E is recommended for analysis using a notch radius equal to 1 mm for any thicknesses of greater than $t \geq 5$ mm without applying any thickness correction for thicker welds. It is worth noting that the notch stress radii captured from the SLIC as-welded samples were found to be in the range of 1.6–5.0 mm, hence greater than the 1 mm baseline recommended in DNV standard. It can be seen in Fig. 7 that while a few of the SLIC data fall upon or above the curve recommended in Appendix E, the majority of data points fall below this recommended curve suggesting that this curve is non-conservative for the SLIC butt welds with the notch radii of greater than 1 mm. Alternatively, further analysis was conducted using

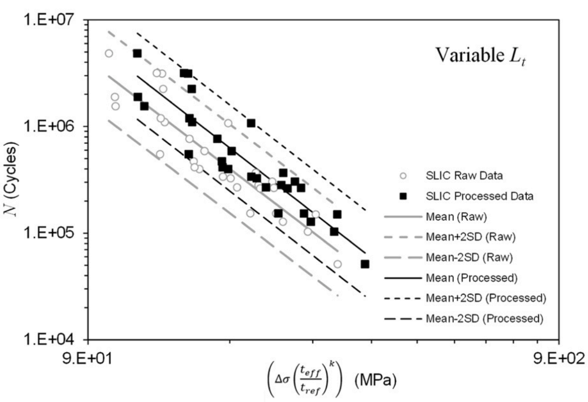

(a)

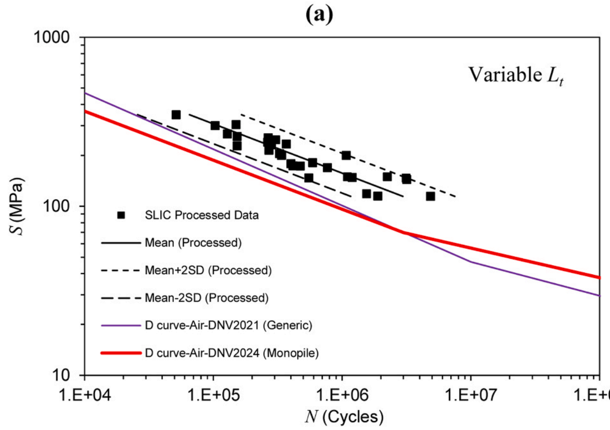

(b)

Fig. 6. (a) Comparison of the SLIC raw data with the processed data using the individual values of L_t and T applied to each of the SLIC test data points, (b) comparison of the regression lines from the processed SLIC data with the fatigue design curves obtained from the old and new editions of DNV-RP-C203 standard.

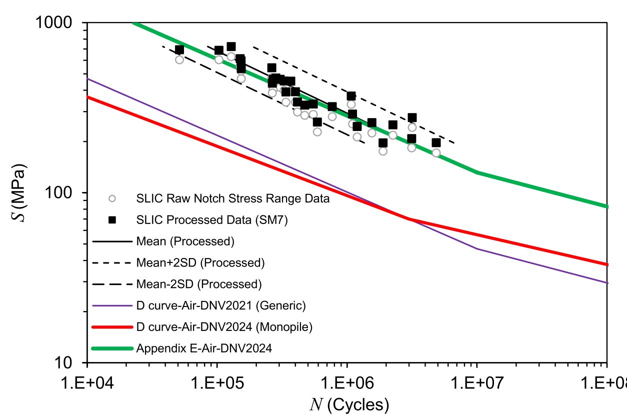

(a)

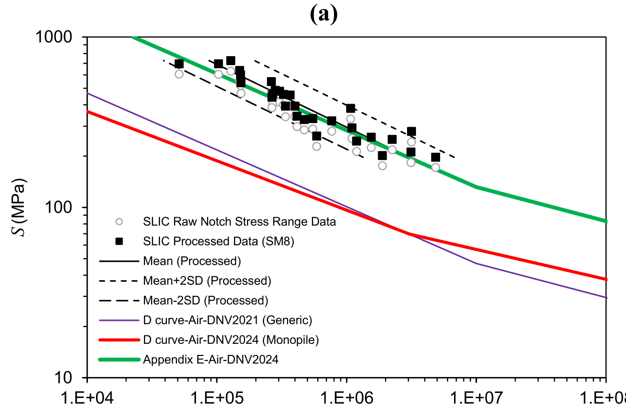

(b)

Fig. 7. Comparison of SLIC raw notch stress range data with (a) the processed data based on SM7 equation, (b) the processed data based on SM8 equation, and also the old and new editions of DNV-RP-C203 standard D curves as well as the recommended curve in appendix E.

the thickness correction approach recommended in the DNV-RP-C203 standard for the D curve. This involved applying processed data by incorporating K_t values at the weld toe regions of as-welded samples and using them as a multiplier in the analysis. The approach is described by the SM7 and SM8 equations, which are provided in Table 4, with the corresponding results presented in Fig. 7(a) and Fig. 7(b), respectively. Moreover, the processed data are compared with the generic and monopile-specific D curves from the old and new editions of DNV-RP-C203 standard as well as the recommended curve in Appendix E from DNV standard and the SLIC raw notch stress range data. Also included in these figures, are the mean and mean$\pm$ 2 SD lines obtained from the linear regression analyses on the processed data based on SM7 and SM8 equations.

It can be seen in Table 4 that employing the K_t values in the regression analysis, enhances R^2 value while considerably decreases the SD value and the magnitude of the inverse slope. Moreover, it can be observed in Fig. 7(a) and Fig. 7(b) that while SM7 and SM8 equations shift up the raw notch stress range data by accounting for the specific weld geometries in each SLIC sample, the mean lines obtained from SM7 and SM8 fall close to the recommended S-N curve in Appendix E. However, the recommended curve in Appendix E of DNV-RP-C203 based on the notch stress analysis is found non-conservative as the mean-2SD lines obtained based on SM7 and SM8 analyses fall underneath it.

It is worth knowing the K_t impact on the S-N design curve for as-welded condition is expected to be embedded in the recommended design D curve in DNV-RP-C203 standard assuming that the welded structures are fabricated in accordance with the DNV guidelines. However, the analysis performed in this study suggests that further work needs to be undertaken to incorporate additional engineering judgments into fatigue design, specifically based on the K_t values at the weld toes, to consider a gradual shift from D curve (i.e. which is suitable for as-welded condition) to C curve (i.e. which is suitable for ground flush condition with zero notch SCF) by considering the quantified value of the notch SCF, rather than following a single D curve for different qualities of weld. Alternatively, further studies can be conducted to revise the recommended curve in Appendix E of DNV-RP-C203 based on the test data on butt welds with the notch radii of greater than 1 mm. This is especially important considering that observations from the SLIC data indicate that samples with large K_t values of higher than the average exhibit a steeper S-N trend with a lower magnitude of m, compared to the rest of the test data points from samples with smaller values of K_t.

The final investigation that is included in Table 4 involves SLIC data processing by accounting for the weld volume (i.e. by multiplying thickness, weld length and weld width) and weld cross sectional area (i.e. by multiplying thickness and weld length). This analysis has been carried out in the absence and presence of K_t, in SM9—10 and SM11—12, respectively. In all analyses conducted using the SM9—12 equations, the individual values of K_t, thickness, weld length, and weld width for each SLIC sample were accounted for and normalised against the reference values established for the baseline dataset with a 25 mm thickness, as detailed in Table 5. As seen in Table 4, the new form of equation based on the weld volume and weld cross sectional area can be also considered in processing of the SLIC data. As seen in this table, in both scenarios of volume and area, the inclusion of the normalised K_t results in lower values of SD and enhanced values of R^2. The comparison of the results obtained with optimum solutions for variable D based on SM9—12 shows that the monopile-specific D curve recommended in the latest edition of DNV-RP-C203 standard falls below the mean-2SD lines obtained from each of these scenarios, indicating that the regardless of the normalisation approach employed in the analysis of the SLIC data, the proposed monopile-specific design curve provides sufficiently conservative fatigue lives compared to the processed SLIC data sets.

According to the procedure described in DNV-RP-C203 standard, the effect of each of the weld parameters on the extent of adjustment in the S-N curve can be separately considered by normalising the weld parameters with respect to the reference values summarised in Table 5, following Eq. 3—Eq. 8. It must be noted that while Eq. 6—Eq. 8 describe the procedure to apply the weld length correction factor on L_{weld} values of greater than the reference value of $l_{weld-ref}$= 100 mm, the SLIC samples had approximately the same weld length as the reference value in DNV standard (see Table 2 and Table 5), resulting in a weld length correction factor of nearly zero.

It is worth noting that the monopile-specific D curve in the standard is meant to provide conservative S-N curves for a wide range of monopile thicknesses and diameters, therefore the sensitivity analysis presented in Table 4 indicates that a richer database on a wider range of thicknesses must be collated in the future to find the optimum values for these constants in order to build a high level of confidence in the design of increasingly larger and thicker monopiles that are commissioned in offshore wind farms.

4. Size effect in butt welds

4.1. Size effect in design standards

The thickness or size effect can be explained by the notch effect at weld toes. The notch effect depends both on the thickness of the plates and the widths of the welds measured as distance between the weld toes. The effect is also dependent on the weld toe angle in addition to weld toe radius. Thus, several geometric parameters may affect the recommended thickness exponent that is also part of this effect. In ISO 19902 [21] the fatigue strength is in general reduced based on thickness only with a thickness exponent of $k = 0.25$ and with reference thickness t_{ref} $= 16$ mm. A similar reduction factor on thickness is presented in EN 1993-1-9 [11] with $k = 0.20$ and $t_{ref} = 25$ mm. The factor on stress increase due to the size effect from these standards are compared with DNV-RP-C203 in Fig. 8.

The size effect based on thickness only was first presented by Gurney in 1979 [22]. 10 years later he included the width of the weld as a parameter in size effect for cruciform joints [23]. The same effect of weld width on size effect was then included in IIW in 1996 [24]. Different expressions for the size effect have been presented in later editions of this document. From Fig. 8 it is seen that the size effect is very different in some design standards, and this effect has significant influence on required amount of steel when large thicknesses are needed. Notably, for plotting the results in Fig. 8, a narrow gap weld groove has been used to derive L_t values for derivation of the weld width following the recommendations in DNV-RP-C203.

4.2. Size effect based on analysis

It is a challenge to derive relevant fatigue data for large thicknesses in the test laboratory; therefore, an assessment of the size effect may be supplemented by engineering analyses. Two types of analyses may be used: effective notch analysis [25] and fracture mechanics such as the procedure presented in [15]. Notch stress analysis of a cruciform joint in [16] indicated that there is an upper limit on effect of thickness around 60 mm on increase in notch stress and thickness effect for a distance between weld toes equal to 50 mm. The weld toe angle used in the analyses in [16] was 45°. Based on the format of the geometry functions presented in [28] for 30° and 45°, it is expected that a similar behaviour will be derived for a similar width in a butt weld with a weld toe angle of 30°, as recommended as the maximum angle in ISO 5817 [26], but with lower calculated notch stresses.

For crack growth analysis using fracture mechanics approach, geometry functions for weld toes with small crack depths are needed. Two different sets of geometry functions for weld toes in butt welds have been previously assessed in the literature [27,28]. The validity range in [28] is broader than in [27]. However, also the minimum crack length normalised by plate thickness a/T value in [28] equal to 0.005 is too

Table 4
Comparison of regression analysis results based on different assumptions employed to generate processed data using the SLIC raw data.

The stress multiplier definition	m	$\log\bar{a}$	$\log a$	$s_{\log N}$	R^2	D
Based on a fixed L_t	3.37	12.989	13.405	0.208	0.82	-
Based on individual values of L_t with a free slope	3.43	13.123	13.527	0.202	0.83	-
Based on individual values of L_t with a fixed slope of $m = 3.45$	3.45	13.176	13.580	0.202	0.83	-
$SM1 = \left(\frac{Min[(14 + DL_t), T]}{t_{ref}}\right)^k$	3.44	13.132	13.533	0.200	0.83	0.60
$SM2 = \left(\frac{Min[(D + 0.66L_t), T]}{t_{ref}}\right)^k$	3.46	13.116	13.510	0.197	0.84	0.00
$SM3 = \left(\frac{Min[(DL_t), T]}{t_{ref}}\right)^k$	3.46	13.173	13.568	0.197	0.84	0.80
$SM4 = \left(\frac{Min[(14 + 0.66(L_{t-old} + D)), T]}{t_{ref}}\right)^k$	3.44	13.144	13.543	0.200	0.83	0.00
$SM5 = \left(\frac{Min[(14 + 0.66L_t), DT]}{t_{ref}}\right)^k$	3.44	13.156	13.556	0.200	0.83	1.11
$SM6 = \left(\frac{Min[(14 + 0.66L_t), T]}{t_{ref}}\right)^D$	3.58	14.518	14.891	0.187	0.85	1.18
$SM7 = K_t\left(\frac{Min[(14 + 0.66L_t), T]}{t_{ref}}\right)^k$	2.74	12.404	12.748	0.172	0.88	-
$SM8 = K_t\left(\frac{T}{t_{ref}}\right)^k$	2.71	12.351	12.701	0.175	0.87	-
$SM9 = \left(\frac{L_t L_{weld} T}{l_{t-ref} l_{weld-ref} t_{ref}}\right)^D$	3.56	14.804	15.176	0.186	0.86	0.64
$SM10 = \left(\frac{L_{weld} T}{l_{weld-ref} t_{ref}}\right)^D$	3.34	13.236	13.658	0.211	0.81	0.50
$SM11 = \left(\frac{K_t}{K_{t-ref}} \times \frac{L_t L_{weld} T}{l_{t-ref} l_{weld-ref} t_{ref}}\right)^D$	3.18	13.529	13.851	0.161	0.89	0.51
$SM12 = \left(\frac{K_t}{K_{t-ref}} \times \frac{L_{weld} T}{l_{weld-ref} t_{ref}}\right)^D$	2.94	12.492	12.840	0.174	0.87	0.68

Table 5
Assumed reference weld parameters for the baseline dataset with 25 mm thickness.

l_{t-ref} (mm)	$l_{weld-ref}$ (mm)	t_{ref} (mm)	K_{t-ref}
20	100	25	2.03

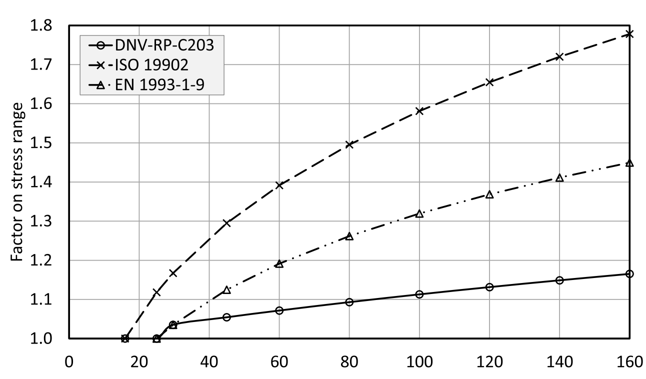

Fig. 8. Comparison of factor for stress increase due to the size effect for butt welds in some standards.

large for performing analysis for large thicknesses. Geometry functions based on [28] are shown in Fig. 9 for different weld toe angles and weld widths for a 50 mm thick plate. It is worth highlighting that accurate values in the geometry function for crack depths of smaller than those shown in Fig. 9 are needed for crack growth analysis. For this purpose a quadratic extrapolation of the function to a crack depth equal to 0.15 mm is performed with the results shown in Table 6. The geometry function for weld notch is assumed to be constant below 0.15 mm [29]. Geometry functions based on [28] were used in [30] to derive the size effect in DNV-RP-C203.

A long semi-elliptic surface crack at the weld toe is assumed for the analysis with initial ratio of half axis $a/c = 0.10$. For a reference thickness equal to $t_{ref} = 25$ mm an initial crack depth of 0.029 mm is calculated for a stress range from the mean D curve at 2 million cycles equal to $\Delta\sigma_{ref} = 122.36$ MPa. Then analyses for a plate thickness equal to 50 mm with weld widths equal to 30 mm and 50 mm were carried out to provide a stress range that corresponds to the same number of cycles of 2 million as shown in Table 6.

Subsequently, the size effect corresponding to the format in the design S-N curve can be derived based on Eq. 9, which follows the same format as Eq. 3:

$$\Delta\sigma_2\left(\frac{t_{eff}}{t_{ref}}\right)^k = \Delta\sigma_{ref} \tag{9}$$

From this equation the following expression for t_{eff} is derived and shown in Eq. 10:

$$t_{eff} = t_{ref}\left(\frac{\Delta\sigma_{ref}}{\Delta\sigma_2}\right)^{1/k} \tag{10}$$

Subsequently, Eq. 11 can be used to estimate parameters in an expression for calculation of the size effect:

$$t_{eff} = Min[(\beta + \alpha L_t), T] \tag{11}$$

For the analysis results in Table 6 it is assumed that $\beta = 14$ mm as used in [13] and the calculated α factors from different crack growth analyses are listed in Table 6.

A thickness exponent of $k = 0.20$ is used for butt welds in DNV-RP-C203 while $k = 0.25$ for cruciform joints where the weld toe angle is typical equal to 40–45° is employed. It is noted that the effective thickness is also a function of the thickness exponent. The calculated results in Table 6 shows that the α factor is dependent on the weld toe

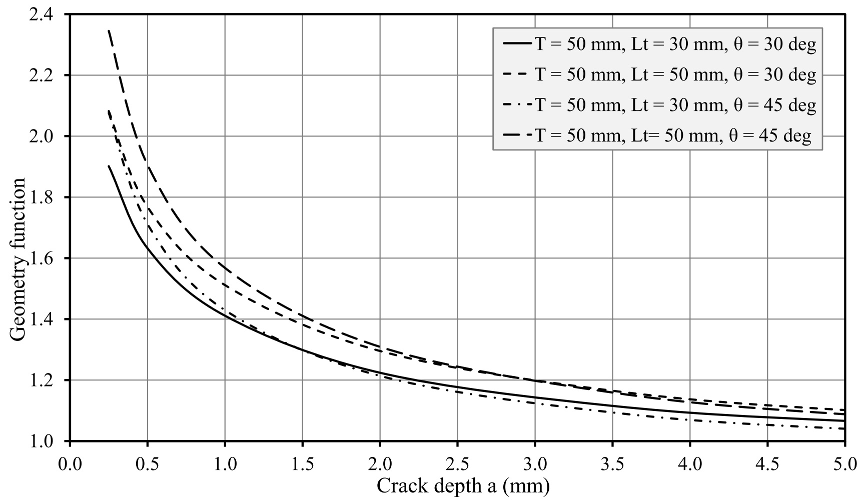

Fig. 9. Geometry function based on the geometry function solutions provided by Bowness and Lee [28].

Table 6
Calculation of size effect factor.

Geometry: $T = 50$ mm	Geometry function at $a = 0.15$ mm	Calculated stress range $\Delta\sigma_2$ at 2 mill cycles	α factor
$\theta = 30^{\circ}$, $L_t = 30$ mm	1.990	121.49	0.39 for $k = 0.20$
$\theta = 30^{\circ}$, $L_t = 50$ mm	2.175	112.54	0.59 for $k = 0.20$
$\theta = 40^{\circ}$, $L_t = 30$ mm	2.132	115.86	0.63 for $k = 0.20$ 0.57 for $k = 0.25$
$\theta = 40^{\circ}$, $L_t = 50$ mm	2.383	108.08	0.54 for $k = 0.20$ 0.65 for $k = 0.25$
$\theta = 45^{\circ}$, $L_t = 30$ mm	2.264	109.55	0.83 for $k = 0.25$
$\theta = 45^{\circ}$, $L_t = 50$ mm	2.548	99.30	0.87 for $k = 0.25$

angle and that the size effect is less for butt welds where the maximum allowable weld toe angle is 30° according to [26].

The formula for the size effect in DNV-RP-C203 with $\alpha = 0.66$ was originally derived for a cruciform joint [30]. Similar values are also derived from the present analyses shown in Table 6. It is worth mentioning that the geometry function for a butt weld is less severe and that a lower reduction factor on fatigue strength may be used for butt welds. However, some of this reduction is already included in a lower thickness exponent for butt welds than for cruciform joints. For thick plates with wide butt welds the weld toe angle may be less than $\theta < 30^{\circ}$. Therefore, it is recommended to use weld geometries from actual production for more refined analysis.. Furthermore, for a better documentation of the size effect based on analysis, improved geometry functions for larger thicknesses are needed.

5. Residual stress effects and potential impact of low R ratio crack growth trends on high-cycle S-N design curve

The fatigue crack growth rate da/dN can be correlated with the stress intensity factor range ΔK using Eq. 12, where C is the power-law coefficient and M is the power-law exponent. The derivation of characteristic S-N curves for butt welds in the high cycle region after the knee point in [15], which explains the procedure developed to derive the monopile-specific D curves presented in the latest edition of DNV-RP-C203 standard, was carried out based on a fracture mechanics-based approach using the recommended fatigue crack growth trends in BS 7910 standard [29]. It is worth noting that there are two sets of fatigue crack growth models presented in BS 7910 standard; one is based on a simplified law, which describes the fatigue crack growth trend using a linear trend in log-log axes, and the other based on a 2-stage law, which describes the fatigue crack growth trend using a bi-linear trend in log-log axes. The model that has been considered and implemented in [15] is the 2-stage law with the mean fatigue crack growth parameters summarised in Table 7.

$$da/dN = C\Delta K^{M} \tag{12}$$

In order to perform the analysis in a conservative manner, it was assumed in [15] that tensile residual stresses induced during the welding process, in a direction parallel to the crack driving force, are present at the weld throughout the entire lifecycle of the OWT monopile support structures. Therefore, to account for the influence of tensile damaging residual stresses in the analysis, the recommended fatigue crack growth trends corresponding to the load ratio of $R \geq 0.5$ from BS 7910 standard were employed in the analysis. While this conservative assumption is normally considered in the design of welded structures, it is well-known that the cyclic loading condition and crack growth process during the operational phase in offshore welded structures may result in redistributed and relaxed profiles of residual stresses depending on actual geometry and long-term loading. Moreover, depending on the soil condition, the chosen pile driving technique (e.g., impact driving, vibratory driving, etc) and the associated load levels, residual stress relaxation may also occur during the installation phase due to pile driving loads and potential bounce-back forces. Additionally, offshore wind designers and operators may explore methods to mitigate

Table 7
Mean crack growth parameters taken from BS 7910 [29] and employed in the analysis.

	Stage A		Stage B		Stage A/Stage B transition point ΔK ($Nmm^{-3/2}$)
R	C	M	C	M	
< 0.5	1.21×10^{-26}	8.16	3.98×10^{-13}	2.88	363
≥ 0.5	4.80×10^{-18}	5.10	5.86×10^{-13}	2.88	196

damaging tensile residual stresses, for example through cost-effective post-weld heat treatment solutions or various surface treatment strategies [31], in the post-fabrication phase and before installation. It should be stressed that these strategies are illustrative, and their actual benefits depend on documented evidence of their effectiveness in reducing or eliminating damaging tensile residual stresses.

As a result of the possible conditions outlined above, assuming that tensile residual stresses constantly remain in offshore wind turbine circumferential welds throughout the entire lifespan of the structures may lead to over-conservatism in the S-N fatigue design process. Therefore, to enable informed engineering judgments based on the residual stress state of real-world assets, and to provide valuable insights for designers aiming to enhance fatigue life and operators targeting optimised asset management decisions for various offshore wind farms, it would be beneficial to reassess the S-N curves by implementing other possible states of residual stresses at the weld toes of monopile support structures. This reanalysis should incorporate more relevant crack growth parameters than those currently available in fatigue design standards. The abrupt change in the crack growth parameters from BS 7910 at $R = 0.5$, as shown in Table 7, is noted. It is expected that the actual physical behaviour of the parameters is more a gradual transition from high R to low R, or more like that of the threshold stress intensity factor range which is presented as a linear function of R in BS 7910. Even with presence of tensile residual stresses at the weld toe, these are reduced at the crack tip as the crack grows into the thickness. Therefore, more accurate crack growth parameters and improved knowledge of residual stresses are important for reliable fatigue life analysis of circumferential welds in monopiles with very large thicknesses.

In this study, following the procedure outlined in [15], the analysis was repeated using the mean fatigue crack growth parameters for a load ratio of $R < 0.5$, as specified in the BS 7910 standard. This approach considers lower tensile residual stresses at the weld toe and is represented by fatigue data sets with relatively low values of load ratio. The result from this analysis gives an increase in allowable stress range by a factor of 1.70 based on $R < 0.5$, which has been illustrated in Fig. 10 for the reference thickness value of 25 mm. In this figure, the fatigue life in the second part of the S-N curve (i.e. the high cycle region after the knee point) is estimated by considering the fatigue crack growth trends corresponding to the load ratio of $R \geq 0.5$ (in the presence of significant tensile damaging residual stresses) and $R < 0.5$ (in the absence of significant tensile damaging residual stresses). Moreover, to generate the bi-linear fatigue curve, two assumptions were made: (a) tensile damaging residual stresses in the SLIC welded samples remained present throughout the tests (denoted as Assumption 1), and (b) these tensile residual stresses were progressively relaxed during the tests (denoted as Assumption 2). These assumptions were necessary due to the absence of residual stress measurements on the SLIC samples before and after testing. For Assumption 1, the same allowable stress range factor of 1.70, which was estimated for the second part of the curve by employing $R < 0.5$ in fracture mechanics analysis, was also applied to the first part. As seen in Fig. 10, applying the allowable stress range factor of 1.70 to the first part (by employing m_1 as a coefficient) and second part (by employing m_2 as a coefficient) of the S-N curve significantly increases the calculated fatigue life by approximately 6 times (×6.2 to be precise) in the first part of the S-N curve and 20 times (×20.6 to be precise) in the second part of the S-N curve. As shown in Fig. 10, for Assumption 2 a more conservative approach was adopted by connecting the point at 10^9 cycles in the second part of the S-N curve from Assumption 1 to the knee point at the end of the first part of the monopile-specific S-N curve (i.e. at $N = 3 \times 10^6$ cycles), which was originally derived using the SLIC data [15]. This approach results in higher intercept and inverse slope values for the second part of the curve, determined as $\log\bar{a}_2 = 29.1307$ and $m_2 = 11.90$, compared to the monopile-specific D curve in DNV-RP-C203 standard. The suitability of each of the two assumptions explained above can be assessed in future work by evaluating the redistribution of residual stresses in the first and second parts of the curve. The effect of residual stresses on fatigue crack growth life is known to be quite substantial as also can be seen where annealed butt welds were tested in [32].

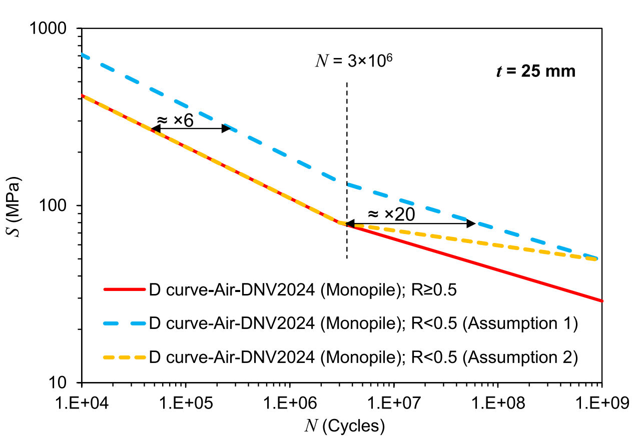

Fig. 10. Illustration of derived S-N curves from different assumptions of residual stresses based on crack growth analyses corresponding to the load ratio of $R \geq 0.5$ (in the presence of tensile damaging residual stresses) and $R < 0.5$ (in the absence of significant tensile damaging residual stresses) with two different assumptions.

It is important to note that while conservatism in the design and operation of offshore wind turbine welded structures can be reduced by considering low residual stress levels (i.e., $R < 0.5$), provided that there is sufficient evidence to justify this assumption for a specific structure, an additional safety factor is typically applied. This is achieved through the use of a design fatigue factor (DFF), which is determined based on the probability of failure. Incorporating DFF in the design process ensures that the structure will achieve its intended lifespan by meeting a specified probability of failure.

6. Discussion and future work

One of the main challenges in enhancing fatigue design curves for increasingly larger and thicker OWT monopile support structures is the lack of fully documented test data on representative welded samples. Such fatigue test data must account for key factors, including: (1) welded samples significantly thicker than 25 mm, which is the reference thickness in the DNV-RP-C203 standard, (2) welds produced using fabrication procedures that replicate those in monopile manufacturing, (3) the use of structural steels employed in monopile fabrication, and (4) well-documented round-robin test programme to ensure data reliability, and preventing results from being solely influenced by a single supplier, fabricator, or test centre. A review of publicly available data reveals that fatigue test data meeting the above requirements are scarce in the open literature. In this regard, the SLIC project provides a valuable resource, as it comprehensively characterises and documents specimen dimensions, weld toe geometries, and misalignment factors through a round-robin test programme involving multiple suppliers, fabricators and test centres. It is important to note that for all 29 SLIC samples tested to completion, the weld height was less than 10 % of the weld width, thereby satisfying the D curve requirements outlined in DNV-RP-C203. Moreover, misalignment factors were individually determined for each test specimen using strain monitoring data obtained from strain gauges attached to opposite sides of the specimens. Furthermore, rigorous quality control was performed post-welding to ensure only specimens with acceptable weld quality and misalignment factors were used in testing. This is reflected in the small misalignment factors across the 29 specimens, ranging from 1.00 to 1.07, with an average value of 1.04. Such comprehensive data, including precise documentation of key variables, is rarely available in historical experimental datasets that were used to derive standard fatigue design curves. Therefore, adopting the detailed procedures established in the SLIC project is crucial for capturing all relevant information in future testing campaigns.

In light of the findings from this study, future research should also focus on evaluating the accuracy of geometry functions used in fracture mechanics to estimate S-N fatigue trends in the high-cycle region. Many historical geometry functions in the literature are limited to specific dimensions, normalised parameters (e.g., crack depth-to-thickness ratio), and geometries (e.g., flat plates or thin pipes). For S-N fatigue analysis, particularly in [15], employing accurate solutions for very small crack depths is critical. This motivates further numerical analysis to develop geometry functions that better represent real-life monopile structures in future work.

Additionally, the accurate characterisation of welding residual stress profiles in monopiles is an area requiring further attention. As demonstrated in Section ↱5, the fracture mechanics-based S-N analysis in the high-cycle region is highly sensitive to whether tensile residual stresses are present or absent at the weld toe in the way the crack growth parameters are presented in the standard for low-stress range intensities. However, there is limited research on the residual stress profiles in monopile weldments. One of the few available studies, which is [33], demonstrates measured residual stresses only along the longitudinal direction in a 90 mm thick monopile weldment, post-welding and before the application of any fatigue cycles. However, due to experimental challenges and time constraint, the residual stresses were not measured in the transverse direction, which is of primary interest for fatigue analysis in the circumferential welds of monopiles. Therefore, further experimental measurements are crucial at various stages of the lifecycle, including post-fabrication, post-installation, and during operation. Such measurements would provide critical insights into residual stress redistribution and relaxation under cyclic loading both in the first part (i.e. with relatively high-stress ranges) and second part (i.e. with low-stress ranges) of the S-N curve. While non-destructive techniques are preferred, the increasing thickness of monopiles presents challenges for non-destructive residual stress measurement which are limited to certain thickness values. Therefore, future research should focus on developing tailored techniques that combine destructive and non-destructive methods to effectively characterise residual stresses in real-life OWT monopiles.

Another pressing need is for more experimental data on double V-grooved butt welds with thicknesses exceeding 50 mm, such as those examined in the SLIC project, especially in the high-cycle region (i.e. second part of the S-N curve). Comprehensive and well-documented round-robin testing programmes can offer valuable insights into the fatigue life of monopiles and reduce excessive conservatism in current fatigue design and life assessment procedures. Considering the high costs and technical challenges associated with fatigue testing of thick welds, it may be wise to keep the reference thickness in design standards at the existing 25 mm. However, a larger experimental database of representative thick butt welds from reliable sources could help develop improved size effect factors, thereby reducing potential errors while maintaining a sufficient level of conservatism in the design of increasingly thicker offshore wind monopile welded structures.

Enhanced fatigue design curves are particularly important for the high-cycle region, which corresponds to the operational cycles experienced by commissioned monopiles nearing the end of their initial design life. Long-term experimental data from variable amplitude fatigue tests, for documentation of the second part of the S-N curve below the fatigue limit, which is observed in constant amplitude tests, can inform procedures for extending the life of existing OWTs and exploring repowering solutions for aged offshore wind infrastructure. Although fatigue testing of thick welded specimens is technically challenging and economically costly due to the need for high-capacity testing machines, such efforts yield invaluable data for optimising fatigue design life, supporting net-zero targets, and reducing the cost of electricity from OWTs by safely extending the operational life of the aged assets.

Finally, while this study focused on S-N fatigue analysis in air environment, future experimental, numerical, and analytical work should address the challenges of fatigue design and life analysis in seawater environments, both with and without cathodic protection. This is particularly important for lifecycle analysis of OWT support structures, accounting for potential damage acceleration due to corrosion at different stages of their lifespan. Combining knowledge of fatigue behaviour in air (as the reference environment) with insights into seawater-induced fatigue will enhance confidence in damage assessments of aged OWT structures and pave the way for robust life-extension solutions for offshore renewable energy assets.

7. Conclusions

This study presents significant advancements in the fatigue design of OWT monopile support structures by addressing critical challenges associated with the increasing size and thickness of monopiles. By leveraging insights from the SLIC project's fatigue data on 50 mm thick as-welded specimens and employing updated fatigue design methodologies, the findings highlight significant improvements offered by monopile-specific D curve introduced in the latest edition of DNV-RP-C203 standard, compared to the generic D curve. Specifically, the analysis demonstrates that at the same stress range level where the fatigue design life based on the generic D curve is 10^7 cycles, the new monopile-specific D curve offers an enhanced life of up to 3.3 times longer for the reference thickness of 25 mm. The study also emphasises the necessity of accurately characterising weld parameters such as weld width, weld length, thickness, and notch stress concentration factors, as these significantly influence fatigue design life as per recommendations in DNV-RP-C203 standard. The sensitivity analysis performed based on realistic values of the weld geometries taken from the SLIC project showed that employing the specific weld geometry for each of the test specimens reduced the standard deviation (hence the level of scatter), increased R^2 value and resulted in an inverse slope of 3.43 which is in very good agreement with the recommended value of 3.45 in the low-cycle region based on the monopile-specific D curve recommendations in DNV-RP-C203. Additionally, the influence of residual stresses on fatigue life was investigated, revealing that assuming tensile residual stresses are negligible at circumferential welds in monopiles during the operational phase increases the allowable stress range by a factor of 1.70 in the high-cycle region. This, in turn, leads to increasing the design life by a factor of up to 20. Future work should address challenges such as expanding the fatigue database for monopile welded structures by testing welded specimens with larger thicknesses in the high-cycle region, refining geometry functions for fatigue crack growth analysis based on realistic as-built weld geometries, improving efficient techniques for measuring residual stress profiles at different stages of the lifecycle, and further investigation on the fatigue behaviour in seawater environments.

CRediT authorship contribution statement

Lotsberg Inge: Writing – review & editing, Writing – original draft, Methodology, Investigation, Formal analysis, Conceptualization. **Mehmanparast Ali:** Writing – review & editing, Writing – original draft, Methodology, Investigation, Formal analysis, Conceptualization.

Declaration of Competing Interest

The authors declare that they have no known competing financial interests or personal relationships that could have appeared to influence the work reported in this paper.

Appendix A. SLIC fatigue raw data on as-welded specimens

Table A1
SLIC fatigue test results on as-welded specimens (taken from [19])

Test Number	Stress range (MPa)	Cycles	Status
1	129.92	2,247,933	Complete
2	147.83	767,916	Complete
3	207.17	282,663	Complete
4	273.94	150,111	Complete
5	178.54	1,076,794	Complete
6	181.28	5,360,000	Suspended
7	221.63	305,111	Complete
8	304.93	51,321	Complete
9	199.01	153,434	Complete
10	150.86	471,655	Complete
11	263.57	103,228	Complete
12	180.78	327,000	Complete
13	186.50	269,429	Complete
14	155.12	400,000	Complete
15	127.96	550,000	Complete
16	99.68	4,860,000	Complete
17	233.37	128,284	Complete
18	129.32	3,137,400	Complete
19	208.93	263,303	Complete
20	102.63	1,892,200	Complete
21	174.16	338,335	Complete
22	151.52	415,000	Complete
23	225.79	152,700	Complete
24	159.01	589,800	Complete
25	102.96	1,550,000	Complete
26	130.94	1,100,000	Complete
27	204.39	368,260	Complete
28	223.21	265,878	Complete
29	99.03	6,199,999	Suspended
30	125.98	3,174,685	Complete
31	128.47	1,196,200	Complete

Data availability

Data will be made available on request.

References

[1] Kaldellis JK, Kapsali M. Shifting towards offshore wind energy—recent activity and future development. Energy Policy 2013;53:136–48.
[2] Santhakumar S, Heuberger-Austin C, Meerman H, Faaij A. Technological learning potential of offshore wind technology and underlying cost drivers. Sustain Energy Technol Assess 2023;60:103545.
[3] Climate Change Act 2008 (2050 Target Amendment) Order 2019.
[4] Suzuki M, Jewell J, Cherp A. Have climate policies accelerated energy transitions? Historical evolution of electricity mix in the G7 and the EU compared to net-zero targets. Energy Res Soc Sci 2023;106:103281.
[5] AR6 budget uplift gives a boost to UK offshore wind potential, Offshore Renewable Energy Catapult, July 2024.
[6] European Commission, 24.10.2023. *Communication From The Commission To The European Parliament, The Council, The European Economic And Social Committee And The Committee Of The Regions: Delivering on the EU offshore renewable energy ambitions*. Office for Official Publications of the European Communities, Brussels, COM(2023) 668 final. Available online: ⟨https://eur-lex.europa.eu/legal-content/EN/TXT/?uri=COM:2023:668:FIN⟩ (accessed on 10 January 2025).
[7] Wind Europe. Latest Wind Energy Data for Europe Autumn 2024. Available online: ⟨https://windeurope.org/intelligence-platform/product/latest-wind-energy-data-for-europe-autumn-2024/⟩ (accessed on 10 January 2025).
[8] Pakenham B, Ermakova A, Mehmanparast A. A review of life extension strategies for offshore wind farms using techno-economic assessments. Energies 2021;14(7):1936.
[9] Anandavijayan S, Mehmanparast A, Braithwaite J, Brennan F, Chahardehi A. Material pre-straining effects on fatigue behaviour of S355 structural steel. J Constr Steel Res 2021;183:106707.
[10] API Recommended Practice 2A-WSD: Planning, designing, and constructing fixed offshore platforms—working stress design, *American Petroleum Institute*, Reaffirmed Edition 2020–09
[11] Eurocode 3: Design of steel structures. *European Standard*, Edition EN 1993-1-9.
[12] BS 7608: Guide to fatigue design and assessment of steel products, *British Standards Institution*, Edition 2014+A1:2015.
[13] DNV-RP-C203: *Fatigue design of offshore steel structures, Det Norske Veritas*, Edition 2024-10.
[14] DNV-RP-C203: *Fatigue design of offshore steel structures, Det Norske Veritas*, Edition 2021-09.
[15] Lotsberg I. Derivation of design SN curves for butt welds in support structures for wind turbines. Mar Struct 2025;102:103795.
[16] Toor, K.K. and Lotsberg, I., 2017, June. Assessment of Fatigue Strength of Welded Connections in Thick Plates. *In International Conference on Offshore Mechanics and Arctic Engineering* (Vol. 57687, p. V004T03A036). American Society of Mechanical Engineers.
[17] Mehmanparast A, Taylor J, Brennan F, Tavares I. Experimental investigation of mechanical and fracture properties of offshore wind monopile weldments: SLIC interlaboratory test results. Fatigue Fract Eng Mater Struct 2018;41(12):2485–501.
[18] Mehmanparast A, Brennan F, Tavares I. Fatigue crack growth rates for offshore wind monopile weldments in air and seawater: SLIC inter-laboratory test results. Mater Des 2017;114:494–504.
[19] Mehmanparast A, Chahardehi A, Brennan F, Manzocchi M. Re-evaluation of fatigue design curves for offshore wind monopile foundations using thick as-welded test specimens. Eng Fail Anal 2024;158:107971.
[20] BS EN 10025-4:2004. Hot rolled products of structural steels. Technical delivery conditions for thermomechanical rolled weldable fine grain structural steels.
[21] ISO 19902 Fixed Steel Structures. 2020
[22] Gurney, T. (1979). The Influence of Thickness on the Fatigue Strength of Welded Joints. Boss'79. *Second int. conf. on behaviour of Offshore Structures*, London, UK.
[23] Gurney T.R. (1989). 'The Influence of Thickness on Fatigue of Welded Joints - 10 years on'. *8th OMAE Conf.*, The Hague.
[24] IIW (1996). Fatigue Design of Welded Joints and Components. Recommendations of IIW Joint Working Group XIII-1539-96/XV-845-96. Edited by A. Hobbacher Abington Publishing, 1996, *The International Institute of Welding.*
[25] Radaj D, Sonsino CM, Fricke W. Fatigue Assessment of Welded Joints by Local Approaches. Second edition. Abington, Cambridge: Woodhead Publishing Limited Abington Hall; 2006.
[26] ISO 5817:2014 Fusion-welded joints in steel, nickel, titanium and their alloys (beam welding excluded). Quality levels for imperfections.
[27] Lie ST, Zhao HS, Vipin SP. New weld toe magnification factors for semi-elliptical cracks in plate-to-plate butt-welded joints. Fatigue Fract Eng Mater Struct 2017;40:207–20.
[28] Bowness D, Lee MMK. Prediction of weld toe magnification factors for semi-elliptical cracks in T-but joints. Int J Fatigue 2000;22(5):369–87.

[29] BS 7910 Guidance on Methods for Assessing the Acceptability of Flaws in Fusion Welded Structures, *BSI*, 2019.
[30] Lotsberg I. Assessment of the size effect for use in design standards for fatigue analysis. Int J Fatigue 2014;66:86–100.
[31] Khajeian A, Mahmoudi AH, Mehmanparast A. Shot peening effects on residual stresses redistribution of offshore wind monopile multi-pass weldments. Mar Struct 2019;66:106–20.
[32] Gericke A, von, Borstel T, Gabriel G, Strandberg M, Henkel KM. Fatigue strength of blast cleaned and stress relief annealed butt joints made of structural steel S355J2 + N for offshore wind support structures. Int J Fatigue 2024:108711.
[33] Jacob A, Oliveira J, Mehmanparast A, Hosseinzadeh F, Kelleher J, Berto F. Residual stress measurements in offshore wind monopile weldments using neutron diffraction technique and contour method. Theor Appl Fract Mech 2018;96:418–27.